In vivo dynamic human retinal blood flow imaging using ultra-high-speed spectral domain optical Doppler tomography

Brian R. White, Mark C. Pierce, Nader Nassif, Barry Cense, B. Hyle Park, Guillermo J. Tearney, Brett E. Bouma

Harvard Medical School & Wellman Center for Photomedicine, Massachusetts General Hospital
50 Blossom St., BAR 724, Boston, MA 02114

Teresa C. Chen

Massachusetts Eye and Ear Infirmary and Harvard Medical School
243 Charles St., Boston, MA 02114

Johannes F. de Boer

Harvard Medical School & Wellman Center for Photomedicine, Massachusetts General Hospital
50 Blossom St., BAR 724, Boston, MA 02114
deboer@helix.mgh.harvard.edu

Abstract: An ultra-high-speed spectral domain optical Doppler tomography (SD-ODT) system is used to acquire images of blood flow in a human retina *in vivo*, at 29,000 depth profiles (A-lines) per second and with data acquisition over 99% of the measurement time. The phase stability of the system is examined and image processing algorithms are presented that allow accurate determination of bi-directional Doppler shifts. Movies are presented of human retinal flow acquired at 29 frames per second with 1000 A-lines per frame over a time period of 3.28 seconds, showing accurate determination of vessel boundaries and time-dependent bi-directional flow dynamics in artery-vein pairs. The ultra-high-speed SD-ODT system allows visualization of the pulsatile nature of retinal blood flow, detects blood flow within the choroid and retinal capillaries, and provides information on the cardiac cycle. In summary, accurate video rate imaging of retinal blood flow dynamics is demonstrated at ocular exposure levels below 600 μW.

OCIS codes: (170.4500) Optical Coherence Tomography; (170.4470) Ophthalmology; (280.2490) Flow Diagnostics; (100.6950) Tomographic Image Processing

References and links

1. R. Candido, T. J. Allen, "Haemodynamics in microvascular complications in type 1 diabetes," Diabetes Metab. Res. Rev. **18**, 286-304 (2002).
2. O. Arend, M. Ruffer, A. Remky, "Macular circulation in patients with diabetes mellitus with and without arterial hypertension," Br. J. Ophthalmol. **84**, 1392-1396 (2000).
3. A. Mistlberger, M. Gruchmann, W. Hitzl, G. Grabner, "Pulsatile ocular blood flow in patients with pseudoexfoliation," Int. Ophthalmol. **23**, 337-42 (2001).
4. G. A. Cioffi, "Three common assumptions about ocular blood flow and glaucoma," Surv. Ophthalmol. **45**, S325-S331 (2001).
5. Y. H. Zhao, Z. P. Chen, C. Saxer, S. H. Xiang, J. F. de Boer, J. S. Nelson, "Phase-resolved optical coherence tomography and optical Doppler tomography for imaging blood flow in human skin with fast scanning speed and high velocity sensitivity," Opt. Lett. **25**, 114-116 (2000).

#3285 - $15.00 US Received November 04, 2003; Revised December 10, 2003

6. Y. H. Zhao, Z. P. Chen, C. Saxer, Q. M. Shen, S. H. Xiang, J. F. de Boer, J. S. Nelson, "Doppler standard deviation imaging for clinical monitoring of *in vivo* human skin blood flow," Opt. Lett. **25**, 1358-1360 (2000).
7. A. M. Rollins, S. Yazdanfar, J. K. Barton, J. A. Izatt, "Real-time *in vivo* color Doppler optical coherence tomography," J. Biomed. Opt. **7**, 123-129 (2002).
8. V. Westphal, S. Yazdanfar, A. M. Rollins, J. A. Izatt, "Real-time, high velocity-resolution color Doppler optical coherence tomography," Opt. Lett. **27**, 34-36 (2002).
9. Z. H. Ding, Y. H. Zhao, H. W. Ren, J. S. Nelson, Z. P. Chen, "Real-time phase-resolved optical coherence tomography and optical Doppler tomography," Opt. Express **10**, 236-245 (2002), http://www.opticsexpress.org/abstract.cfm?URI=OPEX-10-5-236
10. V. X. D. Yang, M. L. Gordon, B. Qi, J. Pekar, S. Lo, E. Seng-Yue, A. Mok, B. C. Wilson, I. A. Vitkin, "High speed, wide velocity dynamic range Doppler optical coherence tomography (Part I): System design, signal processing, and performance," Opt. Express **11**, 794-809 (2003), http://www.opticsexpress.org/abstract.cfm?URI=OPEX-11-7-794
11. S. Yazdanfar, A. M. Rollins, J. A. Izatt, "Imaging and velocimetry of the human retinal circulation with color Doppler optical coherence tomography," Opt. Lett. **25**, 1448-1450 (2000).
12. S. Yazdanfar, A. M. Rollins, J. A. Izatt, "*In vivo* imaging of human retinal flow dynamics by color Doppler optical coherence tomography," Arch. Ophthalmol. **121**, 235-239 (2003).
13. R. Leitgeb, C. K. Hitzenberger, A. F. Fercher, "Performance of fourier domain vs. time domain optical coherence tomography," Opt. Express **11**, 889-894 (2003), http://www.opticsexpress.org/abstract.cfm?URI=OPEX-11-8-889
14. J. F. de Boer, B. Cense, B. H. Park, M. C. Pierce, G. J. Tearney, B. E. Bouma, "Improved signal-to-noise ratio in spectral-domain compared with time-domain optical coherence tomography," Opt. Lett **28**, 2067-2069 (2003).
15. N. Nassif, B. Cense, B. H. Park, S. H. Yun, T. C. Chen, B. E. Bouma, G. J. Tearney, J. F. de Boer, "*In-vivo* human retinal imaging by ultra high-speed spectral domain optical coherence tomography," Opt. Lett. **29**, *in press* (2004).
16. M. Wojtkowski, A. Kowalczyk, R. Leitgeb, A. F. Fercher, "Full range complex spectral optical coherence tomography technique in eye imaging," Opt. Lett. **27**, 1415-1417 (2002).
17. M. Wojtkowski, R. Leitgeb, A. Kowalczyk, T. Bajraszewski, A. F. Fercher, "*In vivo* human retinal imaging by Fourier domain optical coherence tomography," J. Biomed. Opt. **7**, 457-463 (2002).
18. M. Wojtkowski, T. Bajraszewski, P. Targowski, A. Kowalczyk, "Real-time *in vivo* imaging by high-speed spectral optical coherence tomography," Opt. Lett. **28**, 1745-1747 (2003).
19. R. Leitgeb, L. F. Schmetterer, M. Wojtkowski, C. K. Hitzenberger, M. Sticker, A. F. Fercher, "Flow velocity measurements by frequency domain short coherence interferometry," in *Coherence Domain Optical Methods in Biomedical Science and Clinical Applications VI*, V. V. Tuchin, J. A. Izatt, J. G. Fujimoto, eds., Proc. SPIE **4619**, 16-21 (2002).
20. B. Cense, T. C. Chen, B. H. Park, M. C. Pierce, J. F. de Boer, "*In vivo* birefringence and thickness measurements of the human retinal nerve fiber layer using polarization-sensitive optical coherence tomography," J. Biomed. Opt. **9**, *in press* (2004).
21. *American National Standard for Safe Use of Lasers*, (American National Standards Institute, Z136.1, Orlando, 2000).
22. J. F. de Boer, C. E. Saxer, J. S. Nelson, "Stable carrier generation and phase-resolved digital data processing in optical coherence tomography," Appl. Opt. **40**, 5787-5790 (2001).
23. W. Drexler, H. Sattmann, B. Hermann, T. H. Ko, M. Stur, A. Unterhuber, C. Scholda, O. Findl, M. Wirtitsch, J. G. Fujimoto, A. F. Fercher, "Enhanced visualization of macular pathology with the use of ultrahigh-resolution optical coherence tomography," Arch. Ophthalmol. **121**, 695-706 (2003).

1. Introduction

Accurate knowledge of retinal blood flow dynamics is important in not only the treatment but also understanding the pathophysiology of many diseases, including diabetic retinopathy [1,2] and glaucoma [3]. However, current ocular blood flow measurement techniques such as fluorescein angiography and laser Doppler flowmetry (LDF) have been limited by low resolution and poor depth of penetration [4]. Fluorescein angiography is also an invasive technique. A better non-invasive modality of visualizing retinal blood flow is needed to improve both treatment and our understanding of the pathways that lead to disease.

Within the past few years, phase-resolved optical Doppler tomography (ODT) based on time domain OCT (TD-OCT) has proven able to make high-resolution, high-velocity-

#3285 - $15.00 US Received November 04, 2003; Revised December 10, 2003

sensitivity cross-sectional images of *in vivo* blood flow [5-10]. ODT measurements of blood flow in the human retina have been demonstrated [11,12], yet the accuracy and sensitivity is compromised by patient motion artifacts, which can introduce phase inaccuracy and obscure true retinal topography. More recently, spectral domain optical coherence tomography (SD-OCT), also known as Fourier domain OCT (FD-OCT), has demonstrated superior sensitivity over TD-OCT [13,14] by a factor of up to 250 fold [15], allowing ultra-high-speed retinal imaging without compromising image quality [15-18]. This technology has recently been combined with Doppler imaging to measure the velocity of a moving mirror and capillary tube flow [19]. In the current study, we present what we believe to be the first use of SD-OCT for continuous *in vivo* imaging of human retinal blood flow dynamics over a time period of several seconds, with data acquisition over 99% of the measurement time.

2. Methods

The SD-OCT system used in the current study is illustrated in Fig. 1 and was described in depth by Nassif *et al*. [15]. Light from a low-coherence superluminescent diode source (Superlum, Russia) with a spectral full-width at half maximum (FWHM) of 50 nm centered at 840 nm was split between a reference arm and a slit lamp, which delivered the beam into the eye [20]. The optical power incident on the eye was limited by the ANSI maximum permissible exposure to 600 μW [21]. Unlike in standard TD-OCT, the reference arm mirror remained stationary, and the rapid-scanning optical delay line (RSOD) was used only to balance the second order dispersion between sample and reference arms. Light returning from both paths was recombined, collimated, and sent to a high-speed spectrometer consisting of a transmission grating (1200 lines/mm), focusing lens and a 2048 element line scan CCD camera with a dynamic range of 33.1 dB and 10-bit digital output (Basler, Germany). The efficiency of the spectrometer was 28%, defined as the ratio of the optical power detected by the camera to the power exiting the detection arm fiber [15]. The maximum line rate of the camera was 29.3 kHz, providing continuous readout with no active cooling required.

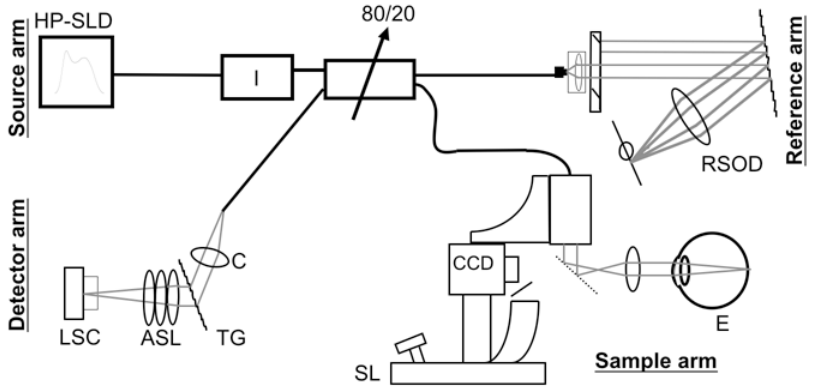

Fig. 1. Diagram of the experimental setup. Light emitted by the broadband source (HP-SLD) passes through an optical isolator (I) and is divided by an 80/20 splitter between a rapid-scanning optical delay line (RSOD) (with stationary mirror) and a slit lamp based telecentric scanner (SL). Returning light is recombined and passed through a collimator (C), a transmission grating (TG), and a three-element air-spaced focusing lens (ASL), before being detected by a line scan camera (LSC).

The detected signal is digitized in ω-space and interpolated to generate a spectrum with points linear in k-space. To remove artifact ghost lines from each frame, all spectra comprising the image are averaged, generating a single background spectrum. Each individual spectrum in the image has this raw background spectrum divided out, and is then multiplied by a smoothed, low-pass filtered background spectrum. This procedure removes

#3285 - $15.00 US Received November 04, 2003; Revised December 10, 2003

all fixed-pattern noise in the image. The resulting spectrum is Fourier transformed to give depth-resolved intensity and phase information, free from artifacts. Due to the ultra-high lateral scan rate (29 frames per second with 1000 A-lines per frame), there is no need for an edge detection algorithm to realign adjacent A-lines, so the true retinal topography is preserved.

A phase-sensitive image is generated by simply determining the phase difference between points at the same depth in adjacent A-lines. This parallels the time domain method pioneered by Zhao *et al*. [5,6]. As with the time domain system, our calculation relies on two assumptions. First, we require that the phase generated by the source is constant from A-line to A-line so that any measured phase differences are due solely to movement within the sample. Second, compared points in adjacent A-lines must be sufficiently close that the speckle at each is reasonably correlated. Adherence to the first assumption is examined in a subsequent paragraph, while assuring that adjacent A-lines are separated by a distance much less than the beam diameter satisfies the second assumption. Here, our acquired A-lines were 1.6 μm apart and the spot size on the retina was estimated to be 30 μm in diameter. Images were typically generated with pixels sized 1.7 μm in depth and 1.6 μm in width, with a depth resolution of 5.1 μm in the retina, assuming a refractive index of $n = 1.38$ [15].

2.1 Phase stability of the SD-ODT system

Accuracy of the phase-sensitive technique is dependent on the phase stability of the system, and this is characterized for our spectral domain system in Fig. 2. Images were captured with a stationary mirror in the sample arm, without scanning the incident beam. Ideally, interference between sample and reference arm light should have identical phase at the mirror position for all A-lines. This condition underlies the assumption that any phase difference between adjacent A-lines is solely due to motion within the sample. The actual phase varies in a Gaussian manner about this ideal, as demonstrated in Fig. 2, where we present the measured probability distribution of phase differences with a standard deviation of $0.296 \pm 0.003°$. This value is over 25 times lower than previously quantified figures for time domain optical Doppler tomography systems [10,22], and at our acquisition speed corresponds to a minimum detectable Doppler shift $f_{D,\min}$ of ± 24.1 Hz, where $f_{D,\min} = \sigma / 2\pi T$ and T is the time between phase measurements (34.1 μs).

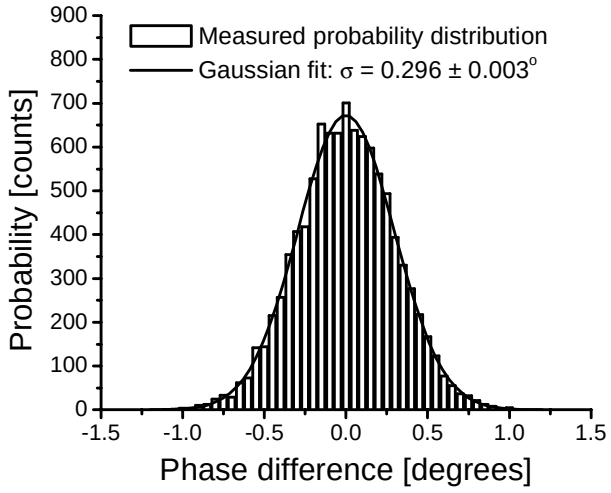

Fig. 2. Probability distribution of the measured phase difference between adjacent A-lines, with a stationary reflector in the sample arm. Bars: Counted phase difference for 9990 A-lines. Bin size = 0.05°. Solid line: Gaussian fit to the distribution, with a measured standard deviation of $0.296 \pm 0.003°$.

#3285 - $15.00 US Received November 04, 2003; Revised December 10, 2003

When finding phase differences, one must recall that complex numbers have unique phase only modulo 2π. Any measured phase differences that have absolute value greater than π must be corrected by a multiple of 2π to lie within this range. This creates a characteristic ring appearance on vessels with high velocities, known as phase wrapping. With a time difference of 34.1 μs between acquired A-lines, phase wrapping occurs at Doppler shifts greater than 14.66 kHz. Thus, the system dynamic range described by the ratio of maximum to minimum detectable Doppler shifts before phase wrapping occurs is over a factor of 600. This improvement is a direct consequence of imaging with a stationary reference arm mirror. Scanning galvanometers used with time domain RSOD mirrors cannot provide perfectly uniform movement, and the associated deviations in angular velocity are a source of phase instability that is not found in spectral domain systems.

The phase information does retain some bulk motion artifacts, from motion of the patient and resonant vibrations of the system. Phase variations due to background motion are an order of magnitude larger than those associated with the inherent phase instability of the system and can obscure true motion in the sample if uncorrected. These artifacts present themselves as slow background trends over the width of a frame. The phase assigned by the Fourier transform to regions of low signal is always zero-mean noise, regardless of background phase difference. Thus, the bulk motion trend is only visible in regions of the retina with significant signal intensity. To remove these trends, the mean phase difference between A-lines i and i+1 (weighted by the corresponding intensity, $I_i(z)$) is removed from A-lines i+1 and greater (as the phase differences are cumulative). For example, let the subscript i denote A-line number while z specifies our position in depth. The phase difference between adjacent A-lines is simply:

$$\Delta\varphi_{i+1}(z) = \varphi_{i+1}(z) - \varphi_i(z) \tag{1}$$

After $\Delta\varphi_{i+1}$ is corrected for phase-wrapping, the bulk motion correction to individual phase values is then given by:

$$\varphi_{i+1,new}(z) = \varphi_{i+1}(z) - \left(\sum_z I_{i+1}(z)\Delta\varphi_{i+1}(z) \right) / \left(\sum_z I_{i+1}(z) \right) \tag{2}$$

These equations assume that φ_i has previously been corrected for the intensity-weighted mean phase difference between it and φ_{i-1}. The new phase values for each A-line are again corrected for phase wrapping. This returns the phases in the low-signal region to zero-mean noise. If phase differences were recalculated without this intermediate step, then bulk motion trends would remain, now present in the low-signal regions. Now, new phase differences are found again between adjacent A-lines, correcting for any phase wrapping. To generate the phase image, a moving box average (MatLab median filter, 5 x 4 pixels, corresponding to an area of 8 x 6.8 μm) is applied to enhance consistent trends and improve the signal to noise. In a final step, the median phase difference of each A-line is subtracted, which corrects for a mean influenced by an area of high flow. The phase-sensitive technique allows visualization of the bi-directional nature of blood flow. To best visualize this feature, the phase images are displayed with a grayscale colormap with white corresponding to $\Delta\varphi = 0.8\pi$ (+12 kHz), black for $\Delta\varphi = -0.8\pi$ (-12 kHz), and gray for $\Delta\varphi = 0$.

3. Results

Images were acquired at 29 frames per second (1000 A-lines per frame) and subsequently processed. The image time of 1/29 Hz = 34.5 ms is slightly longer than the acquisition time for 1000 A-lines at 29.3 kHz (= 34.1 ms), since a finite amount of time is required for the sample arm mirror to return to its original position at the end of each lateral scan. Figure 3 shows a movie of the retina of a healthy volunteer, containing 95 frames acquired in 3.28 seconds. The pupil was not dilated for these measurements. The upper panel shows the intensity image, while the lower panel shows the bi-directional Doppler flow image. The

#3285 - $15.00 US Received November 04, 2003; Revised December 10, 2003

movie is presented at 10 fps, a slower speed than the actual capture rate of 29 fps to allow for visual perception of individual frames. The images are 1.6 mm wide and have been cropped in depth to 580 μm, from their original size of 1.7 mm. The layers of the retina visible in the intensity image have been identified and described previously [23], with the thick, uppermost layer being the nerve fiber layer, and the thinner, strongly scattering deep layer being the retinal pigmented epithelium. Vessel walls are distinct in the phase image, allowing better determination of vessel size and position than may be obtained by identifying shadows cast in the intensity image. There are many notable features within the image. First, note the artery-vein pair on the left-hand side of the image. As the movie progresses over the period of four heartbeats, one can see the pulsatility of blood flow in the artery (a), while the flow in the vein (v) is less variable. Shadowing effects, or low-signal regions, beneath larger vessels are due to the strong signal attenuation in blood relative to surrounding tissue. However, the vessel boundaries are still easily determined in the phase image, and the pulsatile nature of flow is evident. At the lower left-center of the image, it is possible to distinguish blood flow deep within the retina (d). With reference to the intensity image, one can see that this blood flow is being detected *below* the retinal pigmented epithelium, and we believe this is the first time that optical Doppler tomography imaging techniques have been able to observe and localize blood flow within the choroid. To the left of the large vessel on the right-hand side of the image, note the appearance of a very small vessel (c). The diameter of this vessel is slightly under 10 μm (6 pixels by 5 pixels), which is on the same order as the resolution of the system. We believe that this is a capillary, and possibly the smallest blood vessel ever imaged in the retina by Doppler optical coherence tomography.

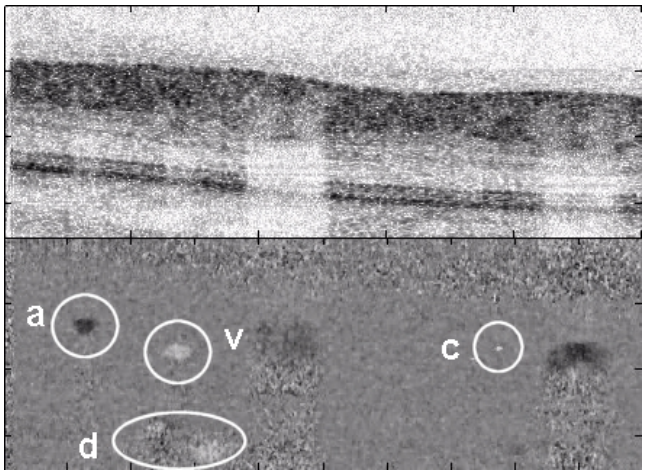

Fig. 3. (1.61 MB) Movie of structure (top panel) and bi-directional flow (bottom panel) acquired *in vivo* in the human eye at a rate of 29 frames per second. The sequence contains 95 frames (totaling 3.28 seconds) played back at a rate of 10 frames per second. Image size is 1.6 mm wide by 580 μm deep. a: artery; v: vein; c: capillary; d: choroidal vessel. (3.82 MB version).

The ultra-high-speed acquisition time of the SD-ODT system allows determination of pulsatile flow dynamics. The identity of vessels in artery-vein pairs can be distinguished, as flow velocity in arteries varies closely with the cardiac cycle, while the blood flow in veins exhibits less fluctuation and lag in phase. Figure 4 presents the phase information from Fig. 3 in a three-dimensional format that more clearly shows the blood flow dynamics. On the *X*- and *Y*-axes are the pixel position (with the upper-left-hand corner of the original image towards us on the left, and the original lower-right on the far back right), while the *Z*-axis provides the Doppler shift at that pixel. To form this image, the phase information of Fig. 3

#3285 - $15.00 US Received November 04, 2003; Revised December 10, 2003

has been spatially averaged over blocks of 16 by 16 pixels, corresponding to an area of 26 μm x 27 μm. As time progresses (at the same slowed rate as in Fig. 3 above), one can distinguish four cardiac cycles. The arteries display negative Doppler shifts, with highly time-dependent velocities. The arterial flow increases dramatically with the onset of the heartbeat, and can subside back to almost zero velocity at the end of the period. This cycle repeats four times over the course of the movie. The veins (including the choroidal flow), which here have positive measured Doppler shift, have less variable flow velocity over the time course of the movie.

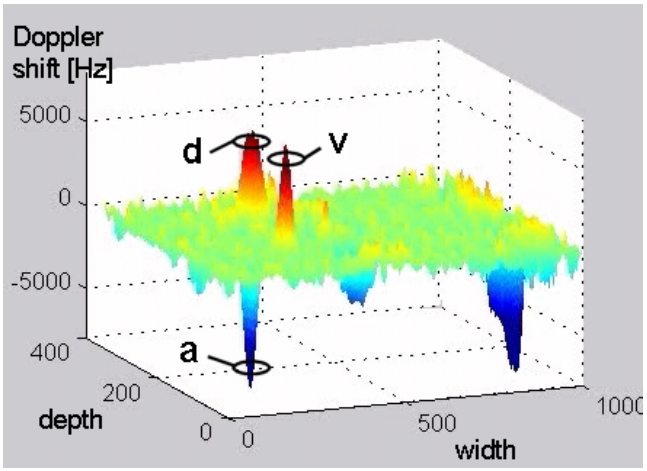

Fig. 4. (1.01 MB) Movie of dynamic blood flow within the human retina, *in vivo*, corresponding to the movie presented in Fig. 3. Image width and depth are mapped onto the *XY*-plane, with Doppler signal [Hz] displayed on the *Z*-axis. Width and depth are denoted in pixels. a: artery; v: vein; d: choroidal vessel.

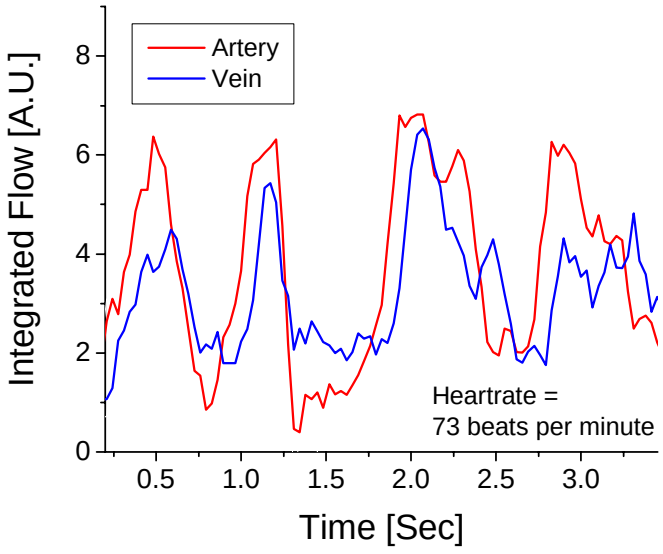

Fig. 5. Integrated flow over the artery-vein pair shown in Figures 3 and 4. A total of 95 frames were acquired at 29 fps, resulting in a total imaging time of 3.28 s.

#3285 - $15.00 US
Received November 04, 2003; Revised December 10, 2003

The retinal blood flow dynamics are further quantified in Fig. 5. The average Doppler shift has been computed at each instant in time over a box of 160 x 170 μm that surrounds the small (~100 μm diameter) artery on the left-hand side of the image. A similar calculation is performed on the adjacent small vein. This average Doppler shift is then graphed over time, with plotted data points representing the mean value from 2 consecutive frames. One can see that flow in the artery follows the expected pulsing pattern. Blood velocity increases rapidly and then slowly decays, repeating four times over 3.28 seconds. Over the same time period, the pulsatile flow effects in the vein are slightly lower and lag in phase with respect to the arterial flow.

4. Conclusions

In summary, we have presented what we believe to be the first application of SD-ODT to continuous *in vivo* human retinal imaging. The ultra-high-speed system offers many advantages in retinal imaging, maintaining high signal to noise while operating at a safe ocular exposure level. Vasculature can be accurately situated in true retinal topography. Large cross-sectional images can be made while retaining high resolution that allows the detection of small blood vessels and capillaries of sizes on the order of 10 μm. SD-ODT also demonstrates the ability to obtain accurate phase information on blood flow from large penetration depths. We were able to detect blood flow below the RPE despite high beam attenuation. The high imaging speed allows detection of pulsatile flow dynamics, distinguishing arteries from veins, and charting velocity throughout a cardiac cycle. We believe these benefits that spectral domain ODT possess over LDF and standard ODT will make it a useful investigational and diagnostic tool.

Acknowledgments

This research was supported in part by research grants from the National Institutes of Health (R24 EY12877 and R01 RR19768), Department of Defense (F4 9620-01-1-0014), and a gift from Dr. and Mrs. J.S. Chen to the optical diagnostics program of the Wellman Center of Photomedicine.

#3285 - $15.00 US Received November 04, 2003; Revised December 10, 2003